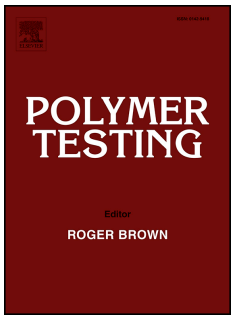

Atomic force microscopy study of polypropylene-based self-reinforced composites

L. Marsich, D. Borin, O. Sbaizero, C. Schmid

PII: S0142-9418(20)30349-4

DOI: https://doi.org/10.1016/j.polymertesting.2020.106632

Reference: POTE 106632

To appear in: *Polymer Testing*

Received Date: 7 February 2020

Revised Date: 23 April 2020

Accepted Date: 16 May 2020

Please cite this article as: L. Marsich, D. Borin, O. Sbaizero, C. Schmid, Atomic force microscopy study of polypropylene-based self-reinforced composites, *Polymer Testing* (2020), doi: https://doi.org/10.1016/j.polymertesting.2020.106632.

L. Marsich: Investigation; Data curation; Formal analysis

D. Borin: Investigation; Data curation; Formal analysis

C. Schmid: Conceptualization; Methodology; Formal analysis; original draft Writing; Funding acquisition

O. Sbaizero: Supervision; original draft Writing – review & editing; Funding acquisition

Atomic Force Microscopy study of polypropylene-based self-reinforced composites

L. Marsich[1§], D. Borin[1§], O. Sbaizero[1], C. Schmid[1]

[§]share authorship

[1] Department of Engineering and Architecture, University of Trieste, 34127 Trieste, Italy

***Corresponding Author**

Prof. Orfeo Sbaizero; Department of Engineering and Architecture; University of Trieste; Via Valerio 10; 34127 Trieste (Italy). Phone +39 040-5583770

Email: sbaizero@units.it

Abstract

Self-reinforced composites are polymeric materials formed by a reinforcement core and a low-melting point skin, which acts as a matrix after the consolidation step. These materials are widely exploited in industrial applications for their mechanical resistance and durability, which are themselves influenced by processing conditions and polymer composition. In the present work, two similar polypropylene-based commercial fabrics were used to evaluate the surface modifications after laminate compaction and after artificial aging using atomic force microscopy. The results were correlated with the chemical and physical-chemical interactions obtained from scanning electron microscopy, transmission electron microscopy, raman and thermal analysis experiments. Single tape consolidated laminate before and after aging displayed different superficial features that can explain the differences in the macroscopic behavior of the two products.

Keyword: Self Reinforced Composites, SRCs, AFM, Raman, Degradation, Thermal analysis,

1. INTRODUCTION

Self-reinforced composites (SRCs) are a promising class of polymers for several industrial applications, such as suitcases, sport equipment, protective armour, automobile parts and road barriers [1,2]. Various manufacturing processes are reported in the literature [1,2], but many researchers have focused their attention on co-extruded tapes made of a highly oriented polypropylene (PP) core and polypropylene/polyethylene (PP/PE) copolymer skin. In this type of material, the core acts as reinforcement and the skin, with lower melting point, becomes the matrix after consolidation.

SRC laminates properties, such as mechanical resistance and durability, are influenced by the drawing process, consolidation parameters, core/skin interface and tape characteristics (e.g., PE content and crystallinity) [3-9]. Utilizing different experimental methods, PP, PE and copolymer PP-PE have examined for both crystallinity determination [6–27] and the influence of fibers on crystallization morphology [28,29]. However, while many studies examine thin film isothermal and non-isothermal melt-crystallisation, in-depth studies concerning the superficial changes that occur as a result of consolidation and artificial aging of SRC are missing. Recently, we reported properties of two commercial self-reinforced polymer composites focusing, in particular, on the peel resistance and on the crystallinity and PE content using the Raman spectroscopy and differential scanning calorimetry (DSC) [30,31]. Considering a possible outdoor application, the effect of UV radiation on the coextruded tape and laminate was also assessed [9,31]. In this case, SRC mechanical properties demonstrated a significant decrease and an evident embrittlement after 250 h of exposure [31]. Fourier-transform infrared spectroscopy (FT-IR) revealed the presence of low molecular weight by-products characterized by carbonyl or hydroxyl/hydroperoxide groups. Their amount was higher in tapes compared to laminates due to internal stresses induced by the drawing process. DSC and FT-IR results proved that the amorphous phase present in laminates is able to rearrange its structure causing an increase in the overall crystallinity. Furthermore, Raman spectroscopy revealed that after prolonged exposure time, photo-degradation induces a rise of the isomeric defect fraction, limiting chemi-crystallisation both for tapes and laminates [31].

Atomic force microscopy (AFM) can be a powerful tool to characterize topography, as well as many other properties of polymer composites. It has several advantages over electron microscopy: (i) samples do not need to be coated as for scanning electron microscopy (SEM) observation; (ii) it does not need ultrathin samples as in the case of transmission electron microscopy (TEM). Furthermore, many composite polymeric materials exhibit nanoscale domains. Assessing the stiffness of such domains can help us understand their contributions to the overall mechanical properties of the bulk materials. The specific goal of this work was to investigate two commercial self-reinforced composites with the same number of tapes arranged in warp and weft directions and in particular to examine the surface changes after compaction and after aging of these materials. Here, we compared AFM results with the chemical and physical-chemical interactions obtained from SEM, TEM, Raman and thermal analysis experiments.

2. MATERIALS AND METHODS

2.1. Materials

Two commercial fabrics with the same number of tapes arranged in warp and weft direction, were used in this study. Sample P refers to a plain weave fabric and sample T indicates a twill weave style. Both tapes have a highly oriented polypropylene (PP) homopolymer core, whereas they differ in skin composition: sample T skin is composed of a polypropylene-polyethylene copolymer (co-PP/PE) while sample P skin is a blend of PE and a copolymer PP-PE (co-PP/PE+PE), as previously established [30].

The comparative analysis between P and T materials was conducted on both tapes - the single element constituting the fabrics - and consolidated laminates, before and after after artificial weathering. Ten fabric layers were consolidated at 140°C with a pressure of 2.2 MPa for 5 min, using a heating rate of 3.8 K/min, and then cooled at 50°C with a cooling rate of 3.6 K/min.

2.2. Artificial weathering

After consolidation, laminates were artificially weathered for 250 h, as previously described [31]. For sample conditioning, a Q-Sun Xenon test Chamber Model Xe-1 equipped with a xenon-arc lamp, which emits radiation from ultraviolet to infrared, was used. A daylight filter guarantees a spectral power distribution (SPD) of 678.8 Wm^{-2} in the range 300–800 nm equivalent to noon summer sunlight. Irradiation in the range of 340 ± 10 nm and temperature control were achieved by an irradiance sensor and an insulated black panel temperature sensor embedded in the chamber. The exposure parameters were selected in compliance with ISO 4892-part 2.

2.3. Atomic Force Microscopy analysis

Morphological and mechanical characterization of all samples was made using both a Solver Pro-M (NT-MDT, Moscow, Russia) and a Nanowizard 4a (JPK, Berlin, Germany) atomic force microscope. In particular, the latter was used in the Quantitative Imaging (QI) mode, allowing a simultaneous collection of sample morphology and stiffness. With this technique, each pixel is probed with a force-deformation curve: the measured height of the sample is defined at 80% of the force set-point (5nN), while the stiffness is expressed as the slope of the loading curve. A cantilever with pyramidal tip (PPP-FM from Nanosensors™, nominal radius of curvature < 10 nm, nominal force constant = 2 N/m) was used and calibrated by the thermal noise method. Scanned portions were selected randomly along the sample, and for each specimen, at least four areas were probed. Test were carried out by selecting at least 3 portions for each area (ridges, center of the spherulite, fibers) and for each portion approximately 50 points were analyzed, thus having a representative description of each element of interest. For both coarse and fine imaging, 256x256 pixels were acquired. Collected images were processed with the JPK Data Processing software (version spm 6-0-4), using both planar and linear fit between scan lines corrections.

The acquired slope from Quantitative Imaging does not consider the vertical displacement of the cantilever while indenting the sample, thus we have further processed the images to calculate the local stiffness in terms of Young's modulus values. For each domain of

interest, four areas of about 50 points were selected, and the experimental curves were fitted with the Hertz model, considering an indentation depth of 2 nm after the contact point. This depth is enough to cover the indentation phase of the sample. Experimental curves with non-convergent fitting were discarded. The obtained data were tested for normality with the Shapiro-Wilk test, and statistical comparisons were made using a Mann-Whitney test between two conditions, or Kruskal-Wallis test with Dunn's correction for multiple comparison. An α value of 0.05 was utilized as the confidence level. Data are graphically reported as box-plots with Tukey representation and significant differences are displayed as * = $p<0.05$, ** = $p<0.005$, *** = $p<0.001$, **** = $p<0.0001$, n.s. = not significant.

2.4. Differential Scanning Calorimetry and Thermogravimetric analysis

Differential scanning calorimetry (DSC) was carried out as reported in [30,31], thermogravimetric analysis (TGA) was performed using a STA 429 EP Netzsch in air with a heating rate of 10 K/min in alumina crucibles until 800°C, and using a sample weight of about 40 mg.

2.5. Scanning Electron Microscopy and Transmission Electron Microscopy

Sample surfaces were inspected with Stereoscan 430 Leica scanning electron microscope (SEM). Transmission electron microscopy (TEM) was performed with a Philips EM208 (images acquisition Olympus Quemesa, 11 Mpix) on tape P embedded in epoxy resin and cut into thin slices. Images were analysed using Image Pro Plus (Media Cybernetics).

2.6. Raman spectroscopy

The Raman spectra were acquired with an InVia Raman microscope (Renishaw, Wotton-Under-Edge, UK), using 785 nm diode laser delivering 250 mW to the sample. The laser was focused by a microscope objective (10x N.A. 0.75) onto the sample. Several spectra on each sample were collected with an acquisition time of 30 s. Raman spectra were analysed using Fityk 0.9.8 [32], fitting the vibrational bands with the Voigt function. The fraction of

the crystalline phase (X^R_c), the isomeric defect phase (X^R_b) and the amorphous phase (X^R_a) were evaluated using the methods described by Nielsen et al. [33].

3. RESULTS AND DISCUSSION

3.1. Tape analysis

After thermogravimetric analysis, the residual mass at 800°C was 4wt% and 2wt% for tape P and T, respectively, indicating that both fabrics contain an inorganic filler.

In Figure 1, the AFM features of tape P are shown. The entire surface has a spherulitic texture valley type centre. As an example, in Figure 1c, the spherulite profile corresponding to the white line indicated in Figure 1a is shown. Furthermore, Figures 1b and 1d illustrate the 2D and a 3D reconstructions of Figure 1a, respectively. The spherulites have a radial lamellar morphology: spherulite average diameter size is 1.96 ± 0.44 μm while, the lamella thickness is roughly 0.34 ± 0.07 μm (this latter data may be slightly overestimated due to the difficulties of assessing a thickness using the AFM technique). Despite the TGA results, there is no evidence on the surface of filler particles. TEM image of a longitudinal tape section (Figure 2) emphasises (i) skin undulation, (ii) the presence of spherulites only in the skin and (iii) inorganic filler particles in the core, indicated by arrows in Figure 2.

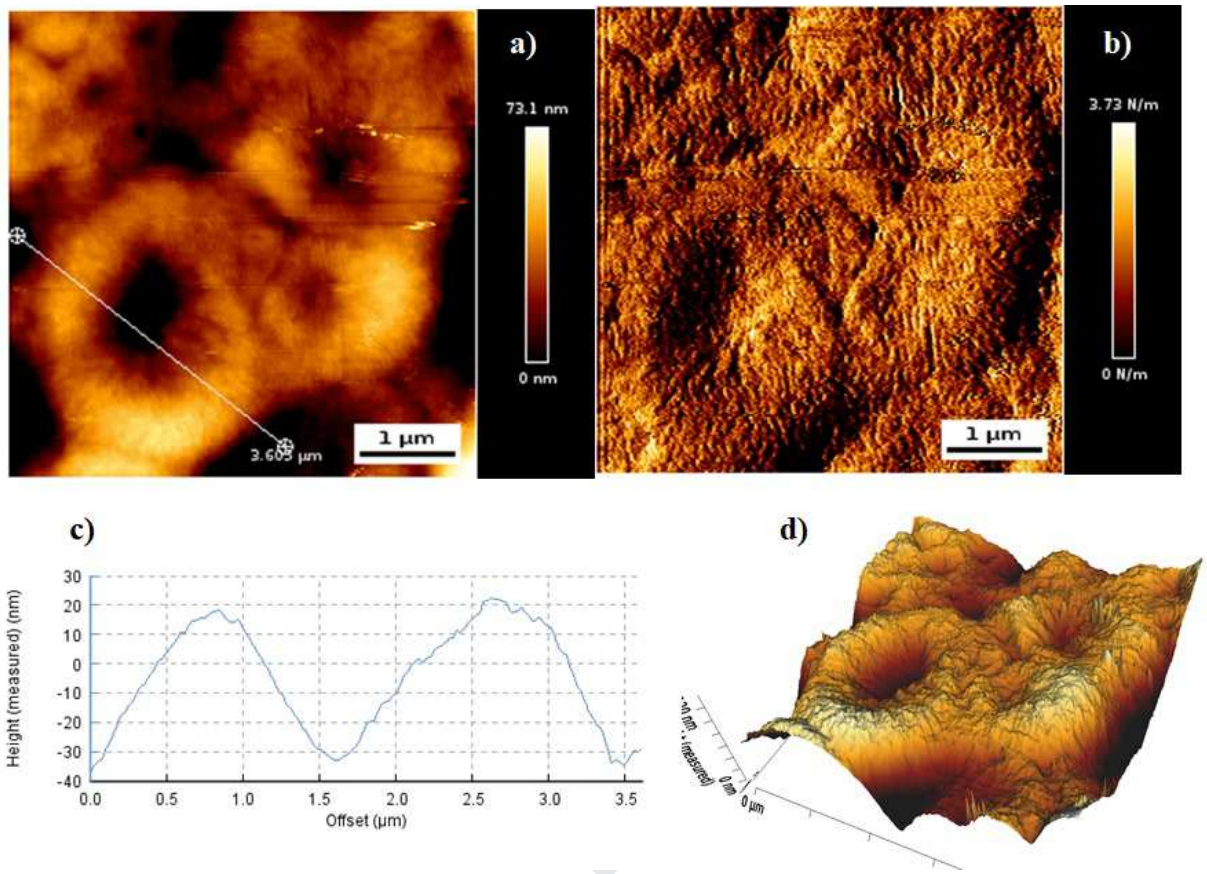

Figure 1. AFM topography of tape P at higher magnification, (a) height mode; (b) force mode; (c) spherulite surface profile measured along the white line in (a); (d) 3D reconstruction of (a).

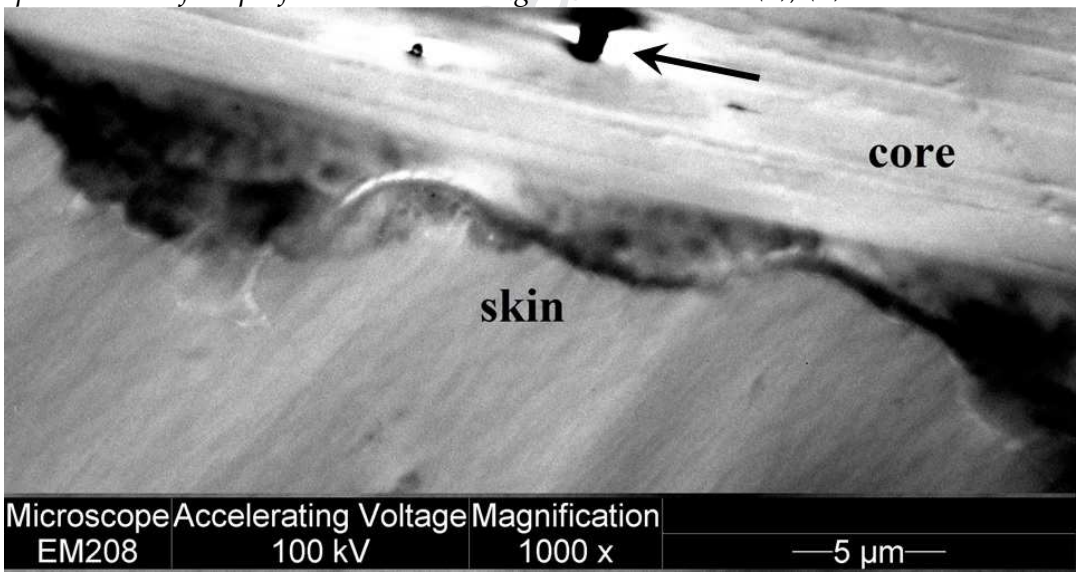

Figure 2. TEM image of a longitudinal section of tape P. Arrow indicate filler particle.

In Figure 3 the AFM results (height and force mode) for T tape are shown. The morphology exhibits a structure with fibres aligned along the direction of tape extrusion and no evidence of spherulites is detected. The presence of areas with a more disordered

structure, as highlighted in Figure 3c and 3d, can be explained by a non-uniform tilting of crystalline portions during the drawing process, as reported by Sauer [34]. In Figure 3 filler particles are also distinguishable as shown by the white circles of panels 3a and 3b.

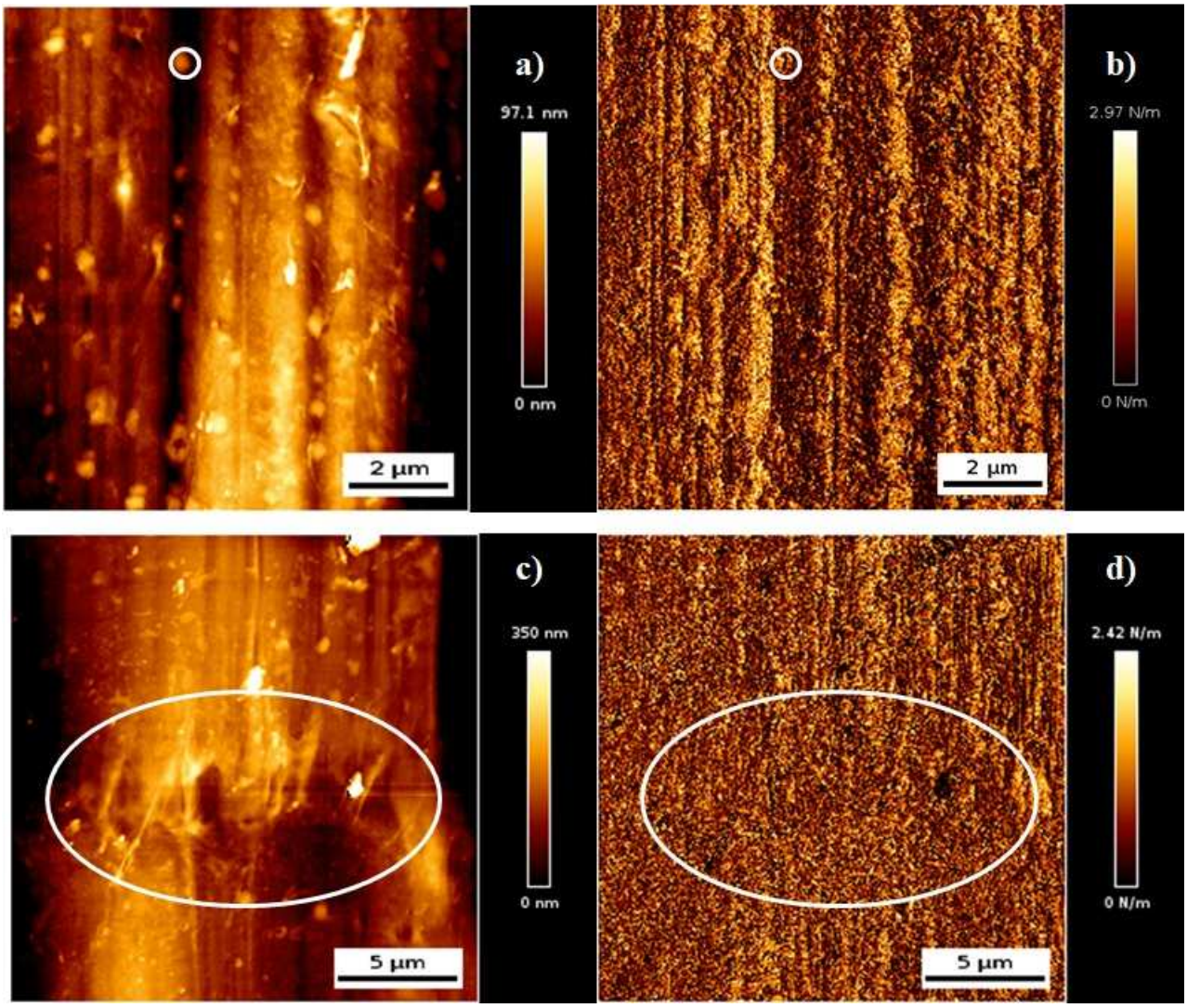

Figure 3. AFM topography of T tape disordered structure; (a) height mode and (b) force mode; (c) and (d) are higher magnifications of panels a and b respectively.)

As revealed by AFM and TEM for sample P, the morphology of the two tapes looks very different. The main reason is the presence of PE only in tape P skin (blend of co-PP/PE+ PE), as demonstrated in [30], with a crystallinity of 38%. Hence the spherulites most likely are due to the PE in the blend which enables crystallization. The non-homogenous skin thickness detected in Figure 2 supports the observation of improper matching of the skin/core viscosities during coextrusion, as previously reported [30].

Conversely, tape T skin is strongly adherent to the highly oriented PP core, according to its profile and therefore does not crystallize into spherulites.

Another consideration regards the filler presence. Fillers were present in the core of both materials, but they are recognizable only on the tape T surface (Figure 3) since, as aforementioned, the skin is strongly adherent to the core.

3.2. Laminate surfaces analysis

In Figure 4, the laminate P surface from the AFM topography is shown. In this case, the spherulitic structure has virtually vanished, and only few features attributable to spherulites are present. This feature probably is due to non-perfect recrystallization during cooling.

In Figure 5a, a SEM image of the P laminate is reported. Some small rods (mean length and width of 411 ± 83 nm and 57 ± 10 nm respectively) are present. For the same specimen, AFM results reported in Figure 5b and 5c show some kind of organization, with lamellae-like dimensions of 560 ± 122 nm and 71 ± 25 nm for mean length and width, respectively comparable to the rods features observed with SEM.

During consolidation, the effects of pressure and temperature are synergic: the skin melts connecting the layers, and the pressure hinders the spherulite formation during cooling. These two phenomena and the low melting PE fraction in the blend of the skin lead to a morphology typical of a skin epitaxial solidification [12] on the isotactic polypropylene (iPP) fibres (not melted) with a knobby structure as also previously reported [35]. Here, the PE lamellae grow on the iPP fibre, and not the γPP on αPP as in Hobbs et al. [35].

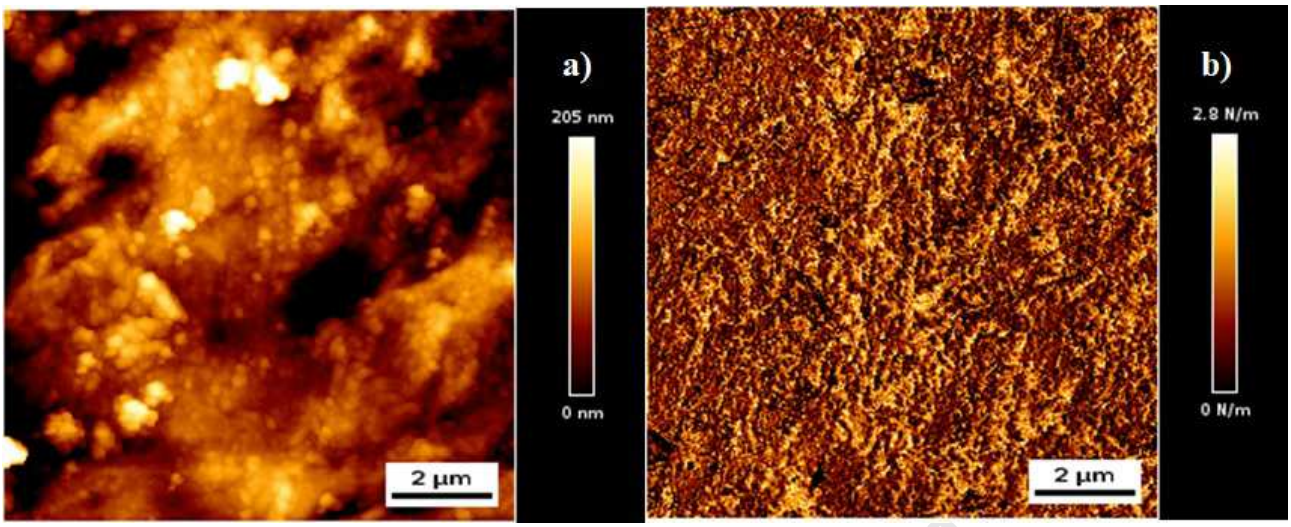

Figure 4. AFM topography of laminate P at higher magnification, (a) height mode and (b) force mode.

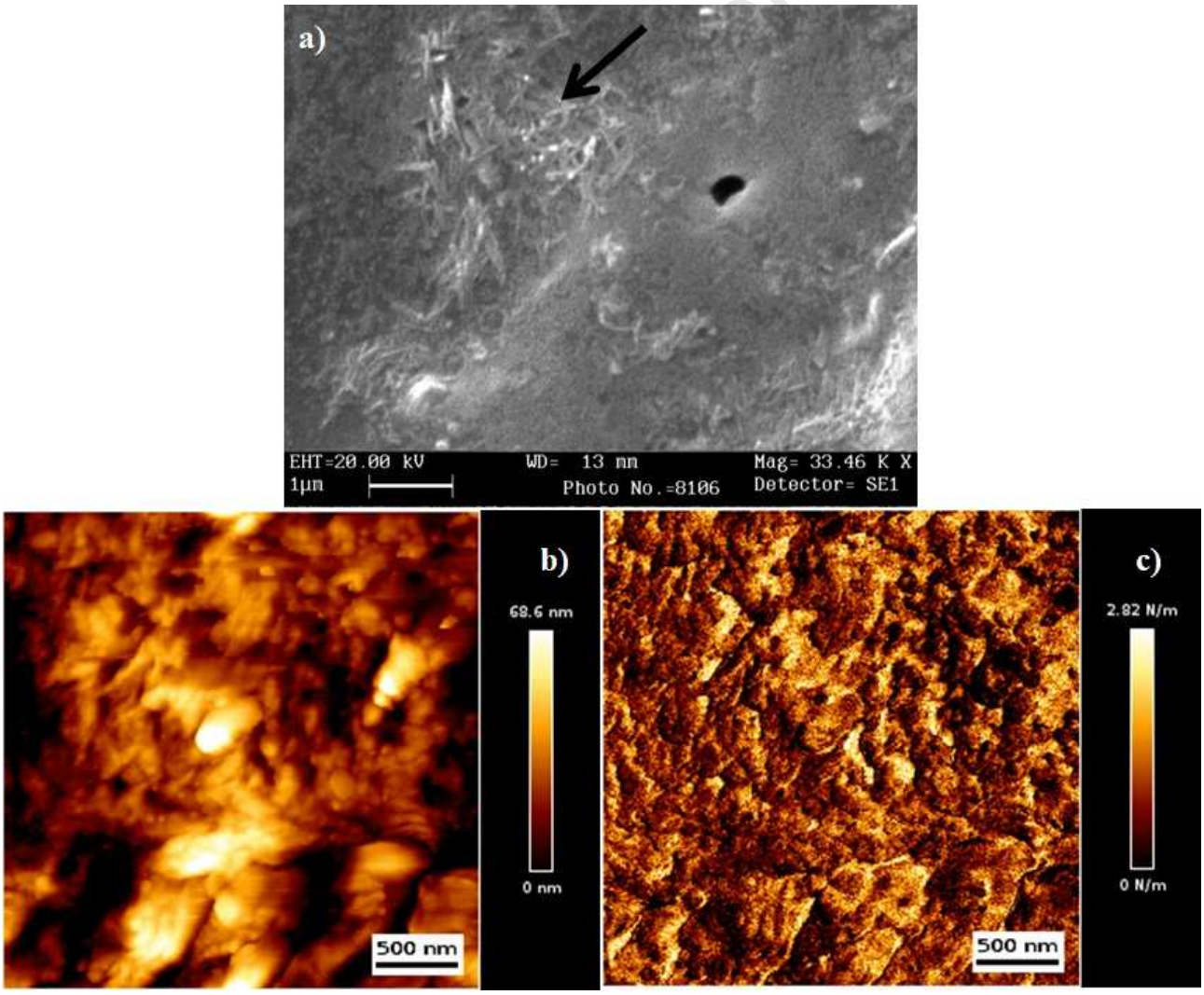

Figure 5. Laminate P surface (a) SEM image; AFM topography at higher magnification (b) height mode and (c) force mode.

Figure 6 shows samples of AFM topographies of the laminate T surface. As in the previous case, there is a joint effect of pressure and temperature during consolidation, which leads, during cooling, to a recrystallization of the skin in a disorganised structure (Figure 6a and b) with no evidence of spherulites, but knobby (Figure 6c and 6d) and "shish-kebab like" (Figure 6e and 6f) structures. The kebab formation is due to lamellar crystallization on pre-crystallized fibres (shish) that act as nucleation sites for the kebabs [29,36-38]. Based on the aforementioned results, we can assume that tape T has a higher iPP core draw ratio than tape P.

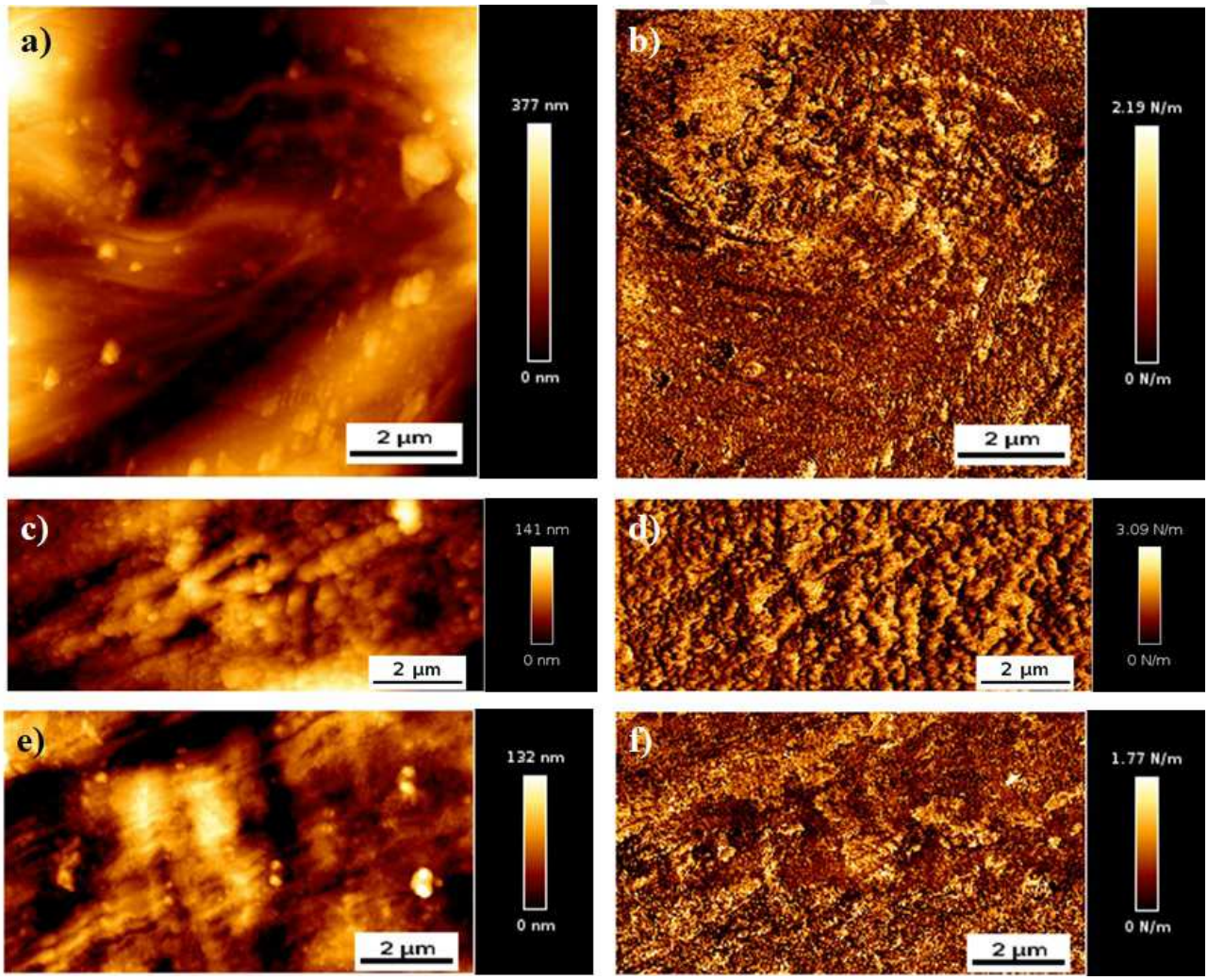

Figure 6. AFM enlargement of laminate T surface: (a), (c) and (e) height mode; (b), (d) and (f) force mode; (a) and (b) disorder; (c) and (d) knobby structure; (e) and (f) shish-kebab like structure.

3.3. Laminate surfaces after aging

After 250 h of exposure both surfaces have developed numerous cracks, as shown in Figure 7 for laminates P and T. It is possible to recognize the tape orientation, since the cracks follow tape extrusion direction. Sample T shows a higher crack density than sample P.

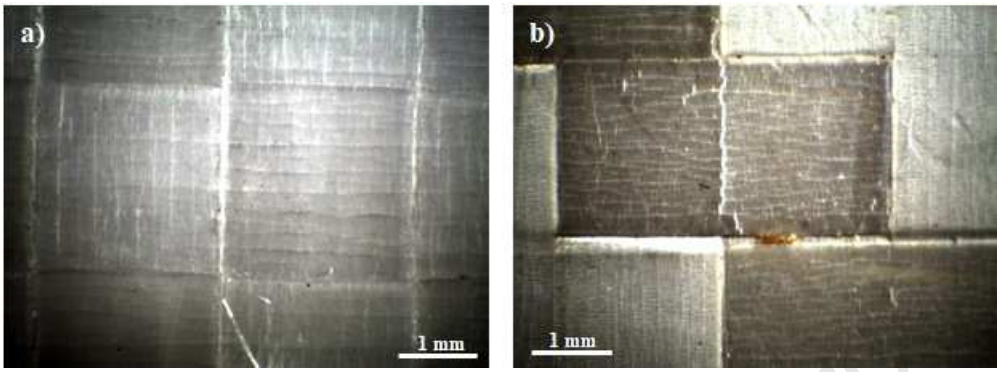

Figure 7. Optical microscope images of (a) laminate P and (b) laminate T surface after 250 h of aging.

3.3.1. Laminate P after aging

In Figure 8, the AFM results for the laminate P after aging are shown. There are obvious crack signs smaller than those visible with optical microscopy (Figure 7a). The crack size ranges from a few microns to millimetres. After aging, spherulites reappear on the surface, more evident around the cracks (Figure 8b). In our previous paper [31], we reported that aging induces an increase in crystallinity due to chemi-crystallization as result of the chain scission. Here, it is evident that the chemi-crystallization happens on the surface skin, forming a spherulite structure due to the PE fraction in the skin, as seen in the tape P. The crystallization produces a shrinkage that promotes a crack formation of microscopic size without orientation. Conversely, macroscopic cracks are oriented along the extrusion direction (the core stretching direction). This orientation is due to the presence of the stretched fibres below the skin that force the skin i) to crystallize and ii) to consequently fracture along a preferred orientation.

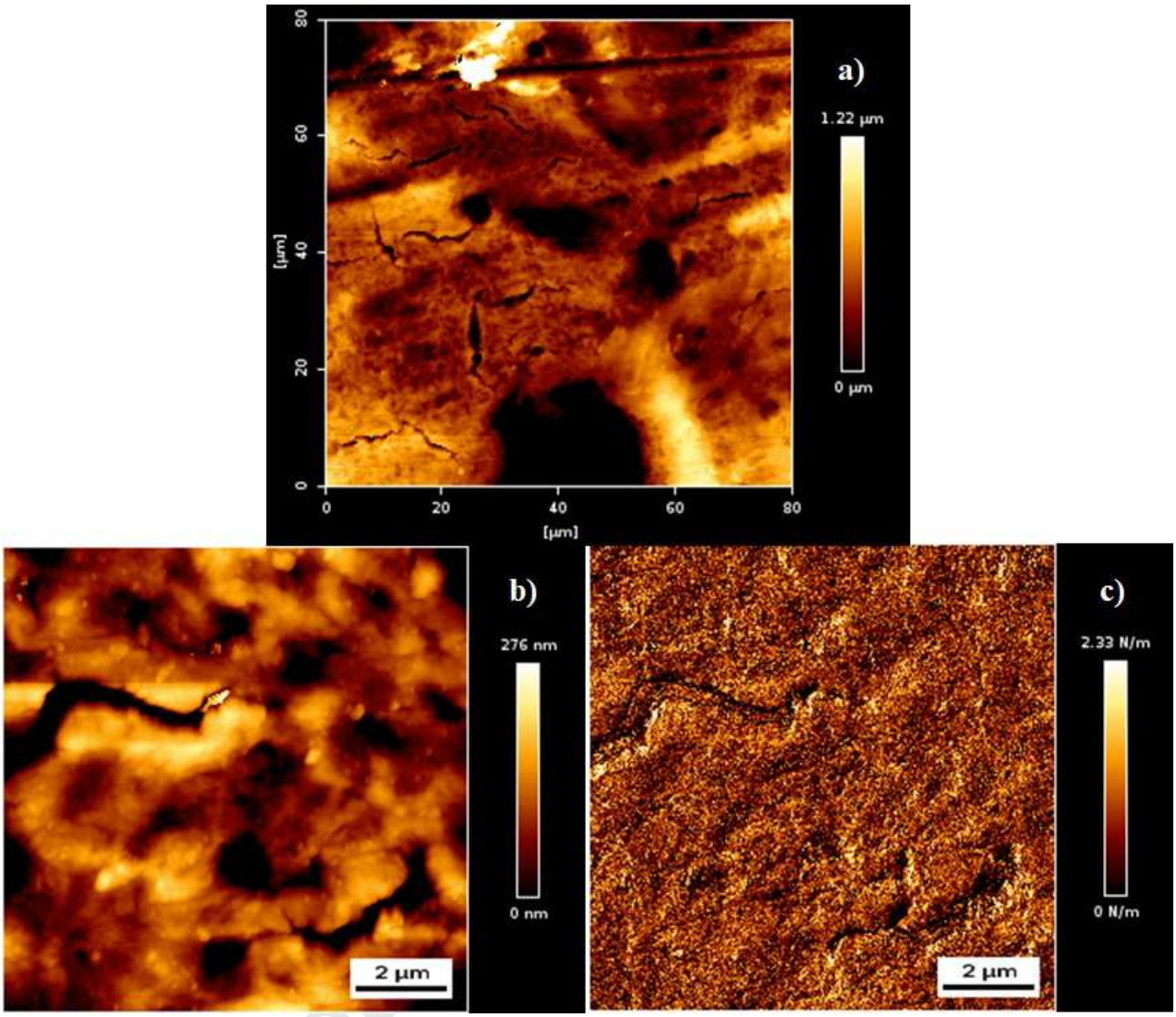

Figure 8. AFM topography of laminate P surface after aging: (a) height mode, the presence of surface cracks is evident; at higher magnification (b) height mode and (c) force mode; there is evidence of spherulitic structure around the cracks.

3.3.2. Laminate T after aging

Figures 9 and 10 show AFM shots of laminate T surface after aging. As found in laminate P, in theT aged laminate surface cracks are evident, oriented along the fibers direction (the tape extrusion direction) (Figure 9). However, unlike the laminate P, in this laminate it is possible to differentiate the iPP fibres under a partially crystallized skin without spherulite formation (Figures 10a and 10c). A one dimensional organized knobby-like structure is also present (Figure 10a). In some areas, larger features with higher density are observed (Figure 10c). In the same picture, on the left side, a crazing feature perpendicular to the

fibres is also present. As described for the laminate P, in laminate T there is an increase in crystallinity, although in this case, the underlying iPP fibres do not seem to be involved in the degradation (at least for the selected aging time). In Figure 10f, zones with increased rigidity are observed that are not detectable using the height mode, probably due to a more closed bundle up of crystal lamellae.

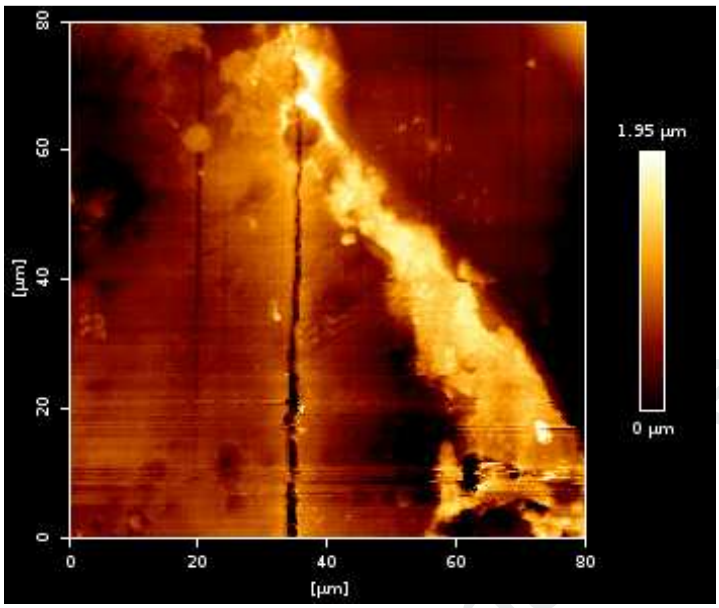

Figure 9. AFM topography of aged laminate T surface.

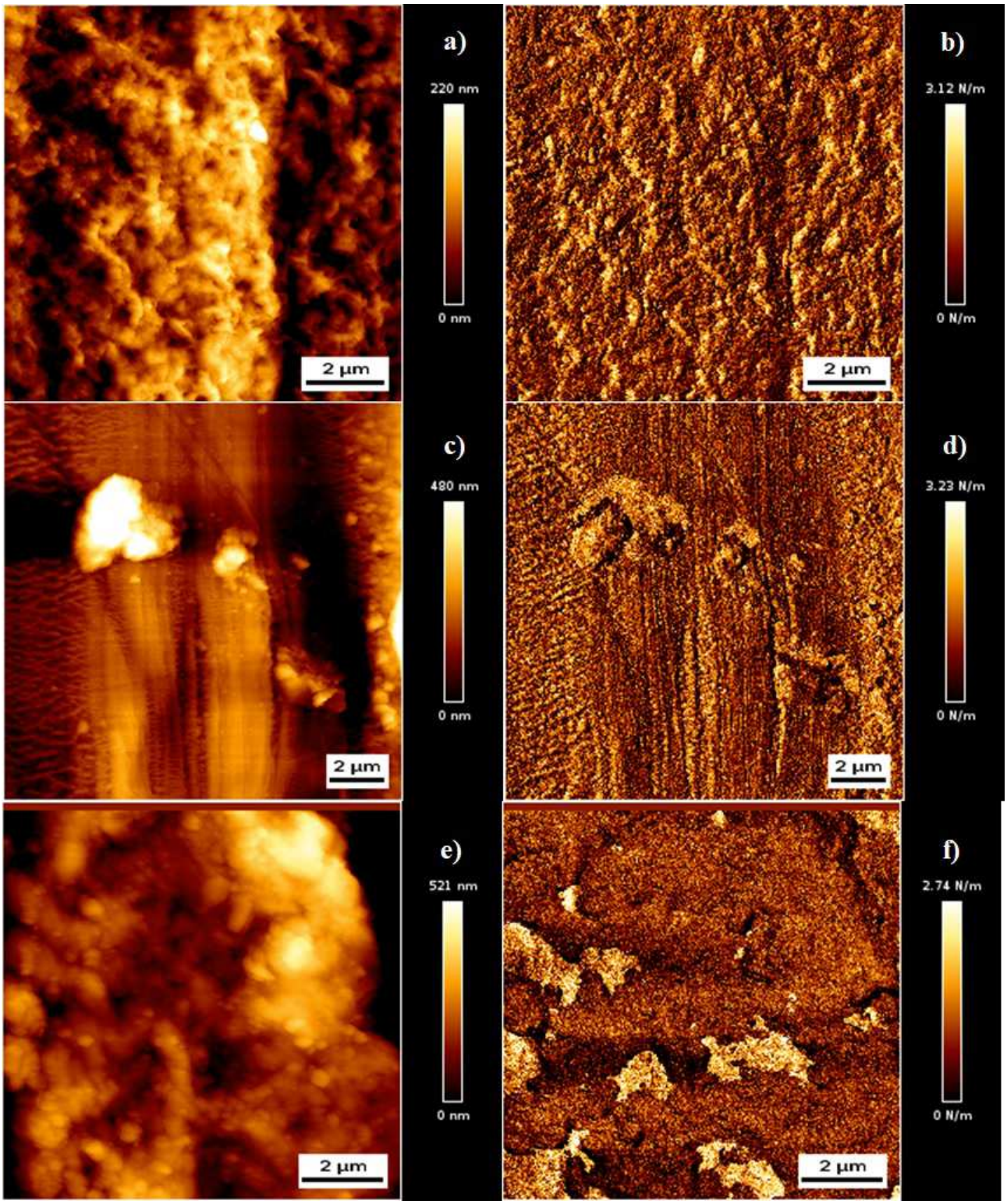

Figure 10. AFM magnification of aged laminate T surface (a), (c), (e) height mode and (b), (d), (f) force mode.

DSC analysis on laminate T before and after the 250 h of aging shows that the crystalline fraction slightly increases from 86% to 88% and the melting peak shifts to a lower temperature (Figure 11a) as has been observed previously [39-45]. The crystallinity

variation for sample P (tape, laminate before and after aging) has already been reported [31]. The Raman spectra are also different (Figure 11b and 11c), showing, after aging, a situation closer to that of the tape. The differences in crystalline fraction for tape and for laminates before and after 250 h of aging as assessed by Raman spectroscopy are reported in Table 1.

The two Raman peaks of Figures 11b and 11c derive from the convolution of 3 peaks: crystalline phase (809 cm^{-1}), amorphous phase (830 cm^{-1}) and the defective phase (840 cm^{-1}), as reported in [30]. It can therefore be seen (Figure 11b) that for the laminate T before aging, the amorphous phase (albeit small - 8% from Table 1) is present (small red peak) as well as the crystalline (51% from Table 1) and defective peaks (41 % from Table 1); on the other hand, after aging the amorphous phase almost disappears (5% from Table 1) and the defective phase is considerably reduced (13% from Table 1) with the result of increasing the crystalline phase from 51% to 82% (Table 1).

Table 1. Calculated fraction of crystalline phase (χ_c^R), isomeric defect phase (χ_b^R), melt-like amorphous phase (χ_a^R) for tape T, laminate before and after 250h of aging time, using Raman spectroscopy.

Phase \ condition	Tape*	Laminate 0h	Laminate 250h aging
χ_c^R (%)	79±1	51±1	82±1
χ_b^R (%)	10±1	41±2	13±0.4
χ_a^R (%)	11±1	8±3	5±1

*Data already published [30]

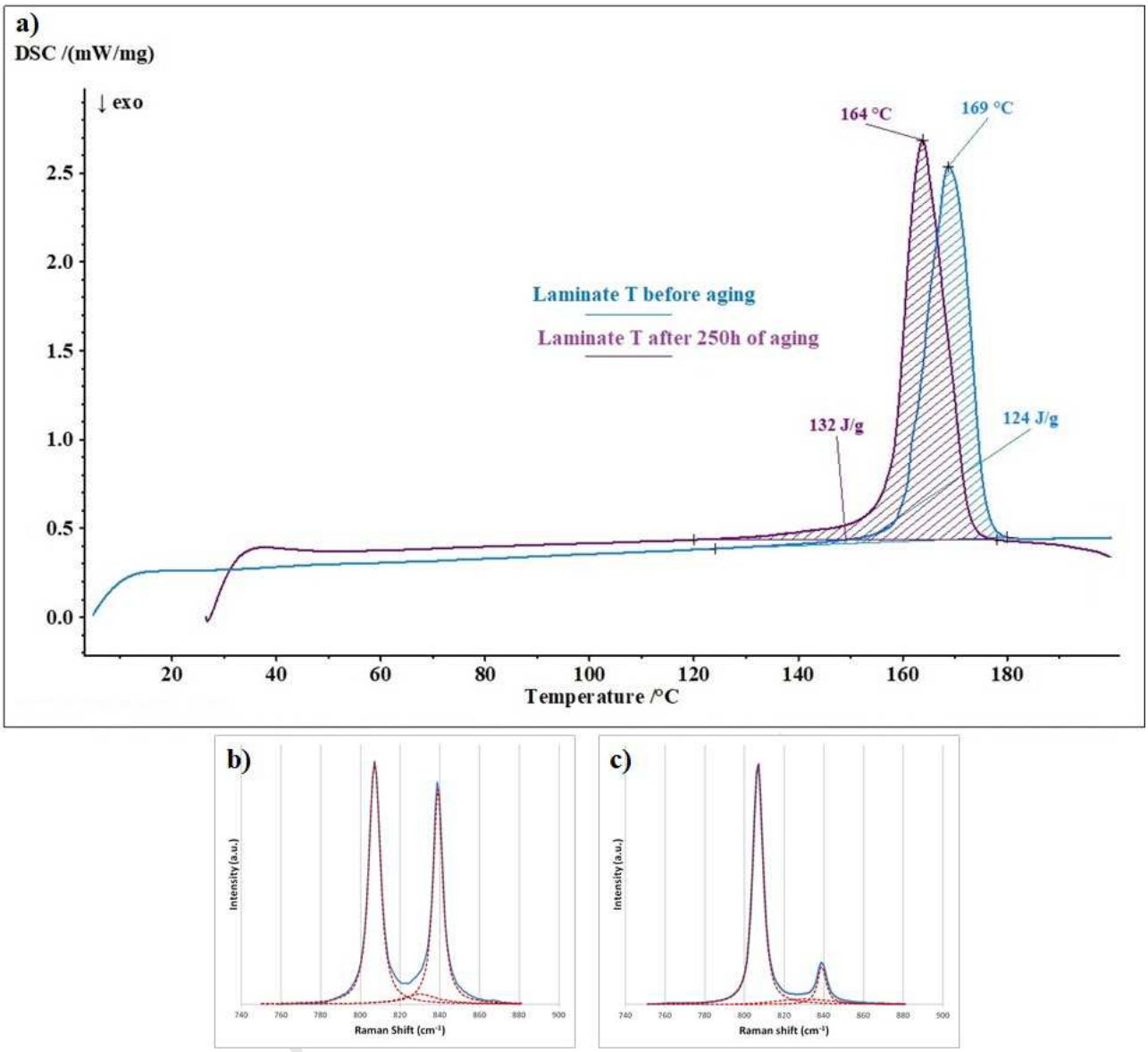

Figure 11. Laminate T: (a) DSC results before and after 250 h of aging. (b) Raman spectra of laminate T before and (c) after aging.

The different results obtained from DSC and Raman on the crystallinity are due to the fact that DSC analysis is volumetric, whereas Raman spectroscopy is focused on the surface. Thus, the higher value found with DSC encompasses the entire iPP-core crystallinity. In this case the crystallinity did not change due to the stretching.

3.4 Young's modulus calculation

In Figure 12, the results for the calculated Young's modulus are reported.

In Figure 12a, the comparison is reported for the bright zone (ridge) of spherulites of tape (Figure 1b), laminate (Figure 4b) and laminate after aging (Figure 8c). As shown from crystallinity results, there is a decrease in E values after lamination and a strong increase after aging.

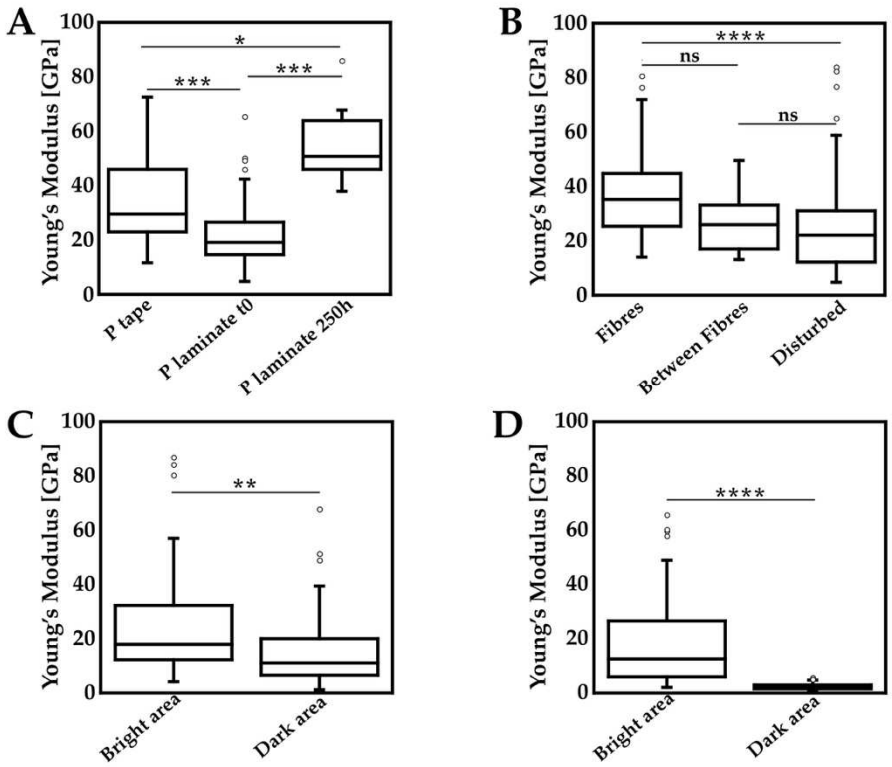

Figure 12. Box plot (a) for the spherulite ridges of P sample; (b) for T tape sample; (c) for laminate T on bright and dark zone of Figure 6; (d) for aged laminate T on bright and dark zone of Figure 10f.

In Figure 12b the comparison among fibre (Figure 3b), between fibre (Figure 3b) and disturbed zone (Figure 3d) for the T tape is reported. There is a decrease in the mean values of the Young's modulus, although not significant, from fibres and zones between fibres, whereas disturbed areas are significantly softer than fibre domains.

For laminate T, the bright areas presented in Figure 6c and 6d (knobby and shish-kebab like structures) are significantly stiffer than surrounding dark domains, as reported in Figure 12c.

After aging of laminate T, very bright zones appear on the surface (Figure 10f) indicating regions that are more rigid than the surrounding areas (Figure 12d).

4. CONCLUSIONS

In the present work, two similar PP based commercial fabrics were used to evaluate the surface modification after laminate compaction and after artificial aging. It should be emphasized that both materials are composed of coextruded tapes made of an iPP stretched core (reinforcement) and a copolymer PP/PE skin with a lower melting temperature (matrix). It is well known that a copolymer iPP/PE can hardly crystallize [46-50]. However, in our study, the P material shows spherulites in both the tape and after aging; the consolidation step destroys the spherulite structure which are not able to form during cooling due to the pressure. This confirms, from a morphological point of view, our previous findings [30] on the composition of the P skin, that it is not only the copolymer but the blend with PE that crystalizes. As expected, the T material did not show spherulites either in tape or in laminate before or after aging, confirming that the skin is effectively a copolymer, well adherent to the stretched iPP core. The consolidation step melts the skin so that it cannot re-crystallize, nevertheless, the non-melted iPP fibres stimulate a shish-kebab like structure.

Aging causes chain breaking and subsequent chemi-crystallisation differently for the two materials. In P there is a restoration of spherulites, while in T, zones with higher stiffness are visible. In both cases, cracks are formed due to re-crystallisation shrinkage, oriented along the extrusion direction. These results lead to the conclusion that between the two materials, the type T, after exposure to UV, shows the greatest signs of embrittlement. Furthermore, the morphology observed in laminate T before and after aging suggests that the iPP core has a higher draw ratio than the P core.

Thus, it can be concluded that the manufacturing process (draw ratio, temperature and time) and the skin composition (copolymer or blend) produce different morphologies both after compaction and especially after aging.

FUNDING SOURCES
The present study was carried out within the INDUSTRIA 2015 – Sustainable Mobility project funded by MISE (Italian Ministry of Economic Development) which the authors would like to thank for financial support.

C. Schmid: Funding acquisition, Conceptualization, Methodology, Writing- Reviewing, , **O. Sbaizero:** Funding acquisition, Conceptualization, Methodology, Writing- Reviewing and Editing **L. Marsich:**, **D. Borin**: Investigation, Validation, Formal analysis, Data curation, Writing- Original draft preparation

§,

DATA AVAILABILITY
All experimental data will be available upon request

References

1. Á. Kmetty, T. Bárány, J. Karger-Kocsis, Self-reinforced polymeric materials: A review, Prog. Polym. Sci. 35 (2010) 1288–1310. doi:10.1016/j.progpolymsci.2010.07.002.
2. J. Karger-Kocsis, T. Bárány, Single-polymer composites (SPCs): Status and future trends, Compos. Sci. Technol. 92 (2014) 77–94. doi:10.1016/j.compscitech.2013.12.006.
3. B. Alcock, N.O. Cabrera, N.-M. Barkoula, J. Loos, T. Peijs, The mechanical properties of unidirectional all-polypropylene composites, Compos. Part Appl. Sci. Manuf. 37 (2006) 716–726. doi:10.1016/j.compositesa.2005.07.002.
4. B. Alcock, N.O. Cabrera, N.-M. Barkoula, A.B. Spoelstra, J. Loos, T. Peijs, The mechanical properties of woven tape all-polypropylene composites, Compos. Part Appl. Sci. Manuf. 38 (2007) 147–161. doi:10.1016/j.compositesa.2006.01.003.
5. B. Alcock, N.O. Cabrera, N.-M. Barkoula, J. Loos, T. Peijs, Interfacial properties of highly oriented coextruded polypropylene tapes for the creation of recyclable all-polypropylene composites, J. Appl. Polym. Sci. 104 (2007) 118–129. doi:10.1002/app.24588.
6. B. Alcock, N.O. Cabrera, N.-M. Barkoula, Z. Wang, T. Peijs, The effect of temperature and strain rate on the impact performance of recyclable all-polypropylene composites, Compos. Part B Eng. 39 (2008) 537–547. doi:10.1016/j.compositesb.2007.03.003.
7. A.Izer, T. Bárány, J. Varga, Development of woven fabric reinforced all-polypropylene composites with beta nucleated homo- and copolymer matrices, Compos. Sci. Technol. 69 (2009) 2185–2192. doi:10.1016/j.compscitech.2009.06.002.
8. B.Alcock, N.O. Cabrera, N.M. Barkoula, T. Peijs, The effect of processing conditions on the mechanical properties and thermal stability of highly oriented PP tapes, Eur. Polym. J. 45 (2009) 2878–2894. doi:10.1016/j.eurpolymj.2009.06.025.
9. Ferluga A, Caniato M, Sbaizero O. The influence of consolidation and artificial weathering on all-PP composite behavior. J Appl Polym Sci 2015;132. doi:10.1002/app.41283.
10. F. Avalos, M. A. Lopez-Manchado and M. Arroyo, Crystallization kinetics of polypropylene: I. Effect of small additions of low-density polyethylene, Polymer Vol. 37 No. 25, pp. 5681-5688, 1996
11. Jun Li, Robert A. Shanks, Robert H. Olley, Giles R. Greenway, Miscibility and isothermal crystallization of polypropylene in polyethylene melts, Polymer 42 (2001) 7685-7694
12. R. Thomann, H. Semke, R.-D. Maier, Y. Thomann, J. Scherble, R. Muelhaupt, J. Kressler, Influence of stereoirregularities on the formation of the γ-phase inisotactic polypropene, Polymer 42 (2001) 4597±4603
13. Jian Li, Chixing Zhou, Gang Wang, Ying Tao, Qing Liu, Yang Li, Isothermal and nonisothermal crystallization kinetics of elastomeric polypropylene, Polymer Testing 21 (2002) 583–589
14. Fajun Zhang, Yumei Gong, Tianbai He, Multiple melting behavior of isotactic polypropylene and poly(propylene-co-ethylene) after stepwise isothermal crystallization, European Polymer Journal 39 (2003) 2315–2322
15. Zhenggang Xiao, Liang Li, Dongshan Zhoua, Gi Xue, Zuanru Yuan, Qingping Dai, Isothermal crystallization of low ethylene content polypropylene random copolymer recovered from decalin and n-hexadecane, Thermochimica Acta 404 (2003) 283–288
16. D. Dudic´, V. Djokovic´ , D. Kostoski, The high temperature secondary crystallisation of aged isotactic polypropylene, Polymer Testing 23 (2004) 621–627
17. Markus Gahleitner, Pirjo Ja¨a¨skela¨inen, Ewa Ratajski, Christian Paulik, Jens Reussner, Johannes Wolfschwenger, Wolfgang Neißl, Propylene–Ethylene Random Copolymers: Comonomer Effects on Crystallinity and Application Properties, Journal of Applied Polymer Science, Vol. 95, 1073–1081 (2005)

18. Jean-Hong Chen, Feng-Chou Tsai, Yu-Hsun Nien, Pei-Hung Yeh, Isothermal crystallization of isotactic polypropylene blended with low molecular weight atactic polypropylene. Part I. Thermal properties and morphology development, Polymer 46 (2005) 5680–5688
19. N. Fanegas, M.A. Go´mez, C. Marco, I. Jime´nez, G. Ellis , Influence of a nucleating agent on the crystallization behavior of isotactic polypropylene and elastomer blends, Polymer 48 (2007) 5324-5331
20. Qamer Zia, René Androsch, Hans-Joachim Radusch, Elisabeth Ingolič, Crystal morphology of rapidly cooled isotactic polypropylene: A comparative study by TEM and AFM, Polymer Bulletin 60, 791–798 (2008)
21. M. van Drongelen, T.B. van Erp, G.W.M. Peters , Quantification of non-isothermal, multi-phase crystallization of isotactic polypropylene: The influence of cooling rate and pressure, Polymer 53 (2012) 4758-4769
22. T. Parenteau, G. Ausias, Y. Grohens, P. Pilvin, Structure, mechanical properties and modelling of polypropylene for different degrees of crystallinity, Polymer 53 (2012) 5873-5884
23. Dimitrios G. Papageorgiou, George Z. Papageorgiou, Dimitrios N. Bikiaris, Konstantinos Chrissafis, Crystallization and melting of propylene–ethylene random copolymers. Homogeneous nucleation and b-nucleating agents, European Polymer Journal 49 (2013) 1577–1590
24. Xiang Zhou, Jiachun Feng, Dong Cheng, Jianjun Yi, Li Wang, Different crystallization behavior of olefin block copolymer in a- and b-polypropylene matrix, Polymer 54 (2013) 4719-4727
25. D. Cavallo, L. Zhang, G. Portale, G.C. Alfonso, H. Janani, R.G. Alamo, Unusual crystallization behavior of isotactic polypropylene and propene/1-alkene copolymers at large undercoolings, Polymer 55 (2014) 3234-3241
26. Alireza Tabatabaei, M. Reza Barzegari, Mohammadreza Nofar, Chul B. Park, In-situ visualization of polypropylene crystallization during extrusion, Polymer Testing 33 (2014) 57–63
27. Yue-fei Zhang, Hui Chen, Bei-bei Liu, Yue-hua Gu, Xiao-xuan Li, Isothermal and non-isothermal crystallization of isotactic polypropylene nucleated with 1,3,5-benzenetricarboxylic acid tris(cyclohexylamide), Thermochimica Acta 590 (2014) 226–231
28. E. Assouline, E. Wachtel, S. Grigull, A. Lustiger, H.D. Wagner, G. Marom, Lamellar twisting in a isotactic polypropylene transcrystallinity investigated by synchrotron microbeam X-ray diffraction, Polymer 42 (2001) 6231-6237
29. Shadi Houshyar, Robert A. Shanks, Morphology, Thermal and Mechanical Properties of Poly(propylene) Fibre-Matrix Composites, Macromol. Mater. Eng. 2003, 288, 599–606
30. Lucia Marsich, Alessio Ferluga, Norman Venturini, Marco Caniato, Orfeo Sbaizero, Chiara Schmid, The Morphological Properties of PP Coextruded Tape Fabrics, (2016) Polym Eng Sci, 56: 727–734. doi:10.1002/pen.24299
31. Lucia Marsich, Alessio Ferluga, Luca Cozzarini, Marco Caniato, Orfeo Sbaizero, Chiara Schmid, The effect of artificial weathering on PP coextruded tape and laminate, Composites: Part A 95 (2017) 370–376
32. Wojdyr M. Fityk: a general-purpose peak fitting program. J Appl Crystallogr 2010;43:1126–8. doi:10.1107/S0021889810030499.
33. Nielsen AS, Batchelder DN, Pyrz R., Estimation of crystallinity of isotactic polypropylene using Raman spectroscopy, Polymer 2002;43:2671–6.
34. Bryan B. Sauer, William G. Kampert, R. Scott McLean, Raisa Monteiro, Thermal Properties and Influence of Orientation on Crystalline Morphologies in Stereoblock Polypropylene and

Related Elastomers, Journal of Polymer Science: Part B: Polymer Physics 2011, 49, 222–243
35. Jamie K. Hobbs, Oliver E. Farrance, Lekshmi Kailas, How atomic force microscopy has contributed to our understanding of polymer crystallization, Polymer 50 (2009) 4281–4292
36. Dukovski and M. Muthukumar, Langevin dynamics simulations of early stage shish-kebab crystallization of polymers in extensional flow, The Journal of Chemical Physics 118, 6648 (2003); doi:10.1063/1.1557473"
37. Robert H. Olley, Geoffrey R. Mitchell, Yasmin Moghaddam, On row-structures in sheared polypropylene and a propylene–ethylene copolymer, European Polymer Journal 53 (2014) 37–49
38. Maria Raimo, On the origin of transcrystalline morphology in polymers and theircomposites: Re-evaluation of different views, Materials Today Communications 3 (2015) 137–140
39. M. S. Rabello and J. R. White, Crystallization and melting behaviour of photodegraded polypropylene– 1. Chemi-crystallization, Polymer Vol. 38 No. 26, pp. 6379-6387, 1997
40. M.S. Rabello, J. R. White, The role of physical structure and morphology in the photodegradation behaviour of polypropylene, Polymer Degradation and Stability 56 (1997) 55-73
41. M. Elvira, P. Tiemblo, J.M. Gomez-Elvira, Changes in the crystalline phase during the thermo-oxidation of a metallocene isotactic polypropylene. A DSC study, Polymer Degradation and Stability 83 (2004) 509–518
42. Iryna Yakimets, Dawei Lai, Miche` le Guigon, Effect of photo-oxidation cracks on behaviour of thick polypropylene samples, Polymer Degradation and Stability 86 (2004) 59-67
43. I.H. Craig, J.R. White, Phua Chai Kin, Crystallization and chemi-crystallization of recycled photo-degraded polypropylene, Polymer 46 (2005) 505–512
44. Fechine GJM, Demarquette NR., Cracking formation on the surface of extruded photodegraded polypropylene plates, Polym Eng Sci. 2008;48:365–72. http:// dx.doi.org/10.1002/pen.20958.
45. Raffaele Gallo, Febo Severini, Course of the changes in thick and thin isotactic polypropylene samples subjected to natural aging, Polymer Degradation and Stability 98 (2013) 1144-1149
46. B. Monasse and J. M. Haudin, Effect of random copolymerization on growth transition and morphology change m polypropylene, Colloid Polym Sci 266:679-687 (1988)
47. Zhenggang Xiao, Liang Li, Dongshan Zhoua, Gi Xue, Zuanru Yuan, Qingping Dai, Isothermal crystallization of low ethylene content polypropylene random copolymer recovered from decalin and n-hexadecane, Thermochimica Acta 404 (2003) 283–288
48. Dimitrios G. Papageorgiou, George Z. Papageorgiou, Dimitrios N. Bikiaris, Konstantinos Chrissafis, Crystallization and melting of propylene–ethylene random copolymers. Homogeneous nucleation and b-nucleating agents, European Polymer Journal 49 (2013) 1577–1590
49. Lei Yu, Tong Wu, Tian Chen, Feng Yang, Ming Xiang, Polypropylene random copolymer in pipe application: Performance improvement with controlled molecular weight distribution, Thermochimica Acta 578 (2014) 43– 52
50. J. Pablo Tomba, Carla D. Mana, C.J. Perez, P. Mariela Desimone, Griselda Barrera Galland, Microstructural characterization of semicrystalline copolymers by Raman spectroscopy, Polymer Testing 52 (2016) 71-78

- 2 commercial SRCs, with the same number of tapes in warp and weft direction were studied
- SRC- type P skin is not only copolymer but blend with PE that crystalizes in spherulites
- SRC – type T skin is a copolymer well adherent to the stretched iPP core and no spherulites
- Manufacturing process and the skin composition produce different morphologies
- The aging causes a chain breaking dissimilar for the two materials

Declaration of interests

☒ The authors declare that they have no known competing financial interests or personal relationships that could have appeared to influence the work reported in this paper.

☐The authors declare the following financial interests/personal relationships which may be considered as potential competing interests: